


Article

Design of Silica Multimode Optical Fibers with Extremely Enlarged Core Diameter for Laser-Based Multi-Gigabit Short-Range Optical Networks [†]

Anton V. Bourdine ^{1,2,*}, Vladimir A. Burdin ¹, Vijay Janyani ³, Ashish Kumar Ghunawat ³, Ghanshyam Singh ³  and Alexander E. Zhukov ¹

¹ Department of Communications Lines, Povolzhskiy State University of Telecommunications and Informatics (PSUTI), 443010 Samara, Russia; burdin@psati.ru (V.A.B.); aadron@bk.ru (A.E.Z.)

² OptoFiber Lab, Skolkovo Innovation Center, 143026 Moscow, Russia

³ Department of Electronics & Communication Engineering, Malaviya National Institute of Technology, Jaipur 302017, Rajasthan, India; vjanyani.ece@mnit.ac.in (V.J.); akghunawat.ece@mnit.ac.in (A.K.G.); gsingh.ece@mnit.ac.in (G.S.)

* Correspondence: bourdine@yandex.ru; Tel.: +78-463-322-161

[†] This paper is an extended version of Zhukov, A.E.; Burdin, V.A.; Bourdine, A.V. Design of silica optical fibers with enlarged core diameter for a few-mode fiber optic links of onboard and industrial multi-Gigabit networks. In Proceedings of the 3rd International Conference Information Technology and Nanotechnology, Samara, Russia, 25–27 April 2017.

Received: 9 September 2018; Accepted: 8 October 2018; Published: 16 October 2018



Abstract: This work presents an alternative fast and simple method for the design of a refractive index profile of silica multimode optical fibers (MMFs) with extremely enlarged core diameters of up to 100 μm for laser-based multi-gigabit short-range optical networks. We demonstrate some results of 100 μm core MMF graded index profile optimization performed by a proposed solution, which provides a selected mode staff differential mode delay (DMD) reduction over the “O”-band under particular launching conditions. Earlier on, a developed alternative model for a piecewise regular multimode fiber optic link operating in a few-mode regime for the computation of laser-excited optical pulse dynamics during its propagation over an irregular silica graded-index MMF with an extremely large core diameter, is utilized to estimate the potentiality of fiber optic links with the described MMFs. Here, we also present the comparison results of the simulation of 10GBase-LX optical signal transmission over 100 μm core MMFs with conventional and optimized graded-index refractive index profiles.

Keywords: laser-based multi-gigabit data transmission; large core multimode optical fiber; few-mode regime; higher-order modes; differential mode delay; mode coupling; on-board cable systems; industrial networks; short-range optical networks

1. Introduction

Nowadays, laser-based optical signal transmission techniques over silica optical fibers with core diameters enlarged in comparison with standard telecommunication single-mode fibers are widely used in various applications of high-bit-rate optical networks. This technique, combined with special launching conditions, provides a few-mode regime, where laser-excited optical emission is transferred over large core optical fibers not by total-mode staff, but only by a limited number of mode components. Since the IEEE 802.3z standard was ratified by the Institute of Electrical and Electronics Engineers (IEEE) in 1998 [1,2], this technique began to be widely used for short-range in-premise multi-gigabit networks, such as cable systems of data and computation centers, storage and local area networks, etc.

Most systems are based on silica-graded index multimode optical fibers (MMFs) with core/cladding diameters of 62.5/125 and 50/125 μm [1–6].

Since 1998, almost every five years, a new-generation of MMFs of Cat. OM2 + OM5 (these categories are outlined and declared in the ISO/IEC 11801 standard ratified by the International Organization for Standardization (ISO) and the International Electrotechnical Commission (IEC)) known as “LOMFs” (laser-optimized multimode-fibers) with a core diameter of 50 μm were specifically developed, designed, and ratified for multi-gigabit optical networks with laser-based transceivers and multimode fiber optic links operating in a few-mode regime [2–4,6].

Nowadays, this technique has become in demand for on-board and industrial network applications requiring 1 Gbps and greater bit rates [7–9], where silica MMFs with enlarged core diameters of up to 100 μm are the most preferable solution. Here, cable systems operate in harsh environmental conditions: high-density mounting spaces, vibrations, dust/suspensions in the air, etc. Therefore, the greater the fiber core diameter, the greater the total network reliability: (a) Optical fibers with a large core diameter of 100 μm (100/125 and 100/140) have almost the same immunity to bending loss as well as specially designed single-mode fibers (SMFs) of ITU-T G.657 Recommendations declared by the International Telecommunication Union—Telecommunication sector (ITU-T) as a solution for indoor “last/first mile” cable systems. (b) Unlike the SMFs of ITU-T G.657 Recommendations, the fiber optic connections of MMFs with a 100 μm core are insensitive to vibrations, and (c) the dust on connector ferrules, due to their great core size. (d) Additionally, the silica core and silica cladding provide lower losses in comparison to the polymer or plastic core/cladding optical fibers. However, the most commercially available MMFs with 100 μm core diameters are targeted only to multimode regimes and are based on multimode light emitting diode (LED) transceivers providing low bit rates of 10–100 Mbps data transmission, while their potentiality for laser-based data transmission in a few-mode regime still requires additional research.

The rest of this paper is structured as follows. Section 2 introduces the features of the DMD effect occurring during laser-excited optical signal transmission over MMFs, presents a brief overview of related works devoted to the design of MMFs with improved bandwidths, and describes in detail the proposed alternative fast and simple method for the optimization of the refractive index profile for MMFs with a reduced DMD, based on an earlier-developed math tool that has been recently modified for the design of 100 μm core MMFs operating under laser-based multi-gigabit short-range optical networks. Section 3 presents an optimized sample of a 100 μm core MMF refractive index profile that provides reduction of DMD over the “O”-band, and some simulation results of 10GBase-LX optical signal transmissions over irregular 100 μm core MMFs with both typical and optimized graded-index refractive index profiles. Section 4 is concerned with discussion that is focused on the analysis of 10GBase-LX channel quality parameters, based on a recalculation of the simulation results, while Section 5 presents our conclusions.

2. Theory

2.1. Related Works

Laser-excited optical signal transfer over MMF by a limited number of mode components primarily differs from a multimode regime by the appearance of the DMD effect [1–6]. DMD is a main issue for short-range multi-gigabit optical networks based on MMFs. Generated by a coherent source, optical emission is launched to an MMF core with a much greater diameter than the laser spot size. This great difference between the fiber core diameter and the laser spot size leads to the excitation of a limited number of particular order modes from the total MMF guided mode staff. Moreover, during propagation in MMF, the amplitudes of these selected mode components transferring the optical signal are non-equal. The description of the amplitude difference is mainly defined by its launching conditions: the typical fiber optic adaptor, radial or angular misalignments, a special matching device, etc. Therefore, the optical pulse at the transmitter end of the fiber optic link contains

several modes with non-equal amplitudes and differing mode velocities (e.g., mode delays). As a result, these modes come to the receiver end with the spread of both amplitudes and delays relative each other, which becomes critical at multi-gigabit rates. DMD strongly distorts the pulse form; it splits at the receiver, and this generates a “glove” effect. Moreover, DMD for each particular “laser–MMF” pair may strong differ, due to the launching uncertainty provided by the variations of sources, connections, and fiber parameters.

A detailed overview of the known solutions concerned with the development of MMF with improved bandwidth is represented in published monographs [10]. Some of them were designed as LOMFs, so that they are targeted not only for modal dispersion reduction, but also for DMD suppression. Most of the known approaches for LOMFs are based on DMD monitoring during fiber preform manufacturing. As proposed in [11–13], the objective function estimates the desired refractive index profile proximity to a profile, which is optimal for the smallest deviation of delays between the total MMF mode staff that satisfies the cut-off condition that corresponds to a multimode regime. In [14–16], the object function is the difference between the integral and the local value of the profile grade parameter α_i for the preform refractive index profile approximated by a simple power function and some optimal α -parameter that is also the best for a multimode regime. Here, local profile-grade parameter correction is performed by reproducing the optimal for the total mode staff DMD diagram—the DMD value distribution on the corresponding mode orders. It is formed by the corresponding modification of the initial DMD diagram of the basic model of optical fibers under overfilled launching conditions, which is the “worst case” for bandwidth, while centralized launching is well known to be the simplest method of implementation under field conditions for bandwidth improvement of a fiber optic link with MMFs operating in a few-mode regime [1,5,10].

Therefore, we suppose that the following outlined factors should be taken into account during the design of MMFs with reduced DMD, or so-called low differential mode delay fibers (LDMDFs) that are optimized for operation under a few-mode regime: (1) Real and approved commercially available LOMFs of Cat. OM2 + –OM5 structure, geometry, refractive index profile, and parameters of data should be used initially/approximated, but not the first generation MMFs of Cat. OM1 and OM2, as well as the model of optical fibers with the ideal graded refractive index profiles as represented by one or a set of simple power-law α -functions. (2) The development or modification of a fiber structure/refractive index profile has to be based on comparison with the DMD diagram. (3) The laser source type and its parameters, including the generated emission initial transverse mode staff and the launching conditions, should be taken into account. (4) Reduced DMD should be provided, not only at particular wavelengths but over the spectral range (for example, conventional telecommunication “O”-band with a reference wavelength $\lambda = 1300\text{--}1310$ nm).

2.2. Design of an LDMDF-Graded Refractive Index Profile

The proposed solution is based on the design of a specialized form of refractive index profile providing a selected guided mode staff delay equalization in relation to some reference delay value, t_{REF} . The designed LDMDF structure weakly satisfies the guiding optical waveguide approximation. It contains a fused silica core doped by germanium and fluorine, bounded by a pure fused silica outer solid cladding. Here, unlike the known solutions, we utilize a stratification method [17] approach to describe the desired refractive index profile. As a result, the designed weakly guiding optical fiber with an arbitrary axially symmetric refractive index profile is represented in the form of a multilayered optical fiber in the core region. It is considered as a finite set on N layers, where the refractive index value stays constant:

$$n(R) = \begin{cases} n_k, & R_k = \frac{k}{N}, 0 \leq k \leq N - 1 \\ n_N, & 1 < R \leq +\infty \end{cases}, \quad (1)$$

and the profile function $f(R)$ describing the refractive index profile by a known relation:

$$n^2(R) = n_{max}^2[1 - 2\Delta \cdot f(R)] \quad (2)$$

is written as follows:

$$f(R) = \begin{cases} h_k, & R_k = \frac{k}{N}, 0 \leq k \leq N - 1 \\ 1, & 1 < R \leq +\infty \end{cases} \quad (3)$$

where $h_k = (n_{max}^2 - n_k^2) / (n_{max}^2 - n_N^2)$ is the local profile parameter; n_k is the refractive index of k layers ($k = 0 \dots N$); n_{max} is the maximal core refractive index; n_N is the outer cladding refractive index; $\Delta = (n_{max}^2 - n_N^2) / 2n_{max}^2$ is the profile height parameter; $R_k = r_k/a$ is the normalized radial coordinate of the k -th layer; r_k is the radial coordinate of the k -th layer; a is the designed LDMDF core radius.

As a result, the desired refractive index profile form in the LDMDF core region is selected in such a way that it should satisfy the minimization of some objective function F described by the proposed simple formula:

$$F = \sum_{j=1}^M (t_{d(j)} - t_{REF})^2 \quad (4)$$

where $t_{d(j)}$ is the desired value of delay for the j -th guided mode $LP_{lm(j)}$ computed at the corresponding synthesis iteration; t_{REF} is some reference value of mode delay that is applied for DMD diagram equalization; M is the total number of the mode components transferring a laser source excited few-mode optical signal with a normalized amplitude that is not less than $A_j > 0.1$, and with a core power (known also as an optical confinement factor) that is not less than $P_{co}^{(j)} \geq 0.5$. Here, the total number of modes M taken into account depends on the following factors: (1) the designed fiber basic geometry parameters (e.g., core diameter and profile height parameter), (2) the launching conditions, (3) the emission of the initial transverse mode staff at the laser output defined by the type of source—vertical surface-emitting laser (VCSEL) or single-mode laser, e.g., Fabry–Perot laser diode (LD)/distributed feedback laser (DFB-laser), and (4) the prediction of a new guided mode of excitation, with $A_j > 0.1$ during the following optical signal propagation over MMF, due to mode mixing and power diffusion effects provided by real fiber irregularities and its micro-/macro-bends and tensions/stress occurring under fiber optic cable manufacturing, installation, and maintenance. Unlike the known solutions, we propose setting the reference delay t_{REF} from the range of values containing the DMD diagram formed for only M selected guided modes, with particular orders propagating in the new generation of LOMFs of Cat. OM2 + –OM4. The objective function F in Equation (4) is minimized by the Nelder–Mead simplex method, whose efficiency was demonstrated in [18,19] concerned with the design of optical fibers.

2.3. Extension of Modified Gaussian Approximation

During objective function (4) minimization, a direct problem of the optical fiber with the current refractive index profile should be solved during each iteration. Here, objective function arguments are an array of local parameters h_k that completely describe the optical fiber refractive index profile. Therefore, a fast and simple method for the computation of both the fundamental and higher-order mode parameters propagating in MMF is required. We propose utilizing earlier on the developed modification of a Gaussian approximation [20] that is generalized and extended [21] for the evaluation of arbitrary order-guided mode dispersion parameters propagating in a weakly guiding optical fiber, with an arbitrary axially symmetric refractive index profile in the core region, bounded by a single solid outer cladding. This extended modified Gaussian approximation (EMGA) is based on a combination of “classical” Gaussian approximation [22] and a stratification method [17] for the researched MMF complicated graded refractive index profile representation. The proposed approach permits the derivation of an analytical formula for the square core mode parameter U^2 in the form of finite nested sums [21] from a well-known integral variational expression [22]:

$$U^2 = \frac{(m - 1)!}{(l + m - 1)!} \left\{ \frac{Q}{R_0^2} + V^2 \left[X_0 + \sum_{k=0}^{N-1} h_k (X_1 - X_2) \right] \right\} \quad (5)$$

where

$$\begin{aligned}
 X_0 &= \exp\left(-\frac{1}{R_0^2}\right) \sum_{q=0}^{2m-2} D_q \sum_{p=0}^{l+q} \frac{(l+q)!}{p!R_0^{2p}} \\
 X_1 &= \exp\left(-\frac{k^2}{N^2R_0^2}\right) \sum_{q=0}^{2m-2} D_q \sum_{p=0}^{l+q} \frac{(l+q)!}{p!R_0^{2p}} \frac{k^{2p}}{N^{2p}} \\
 X_2 &= \exp\left(-\frac{(k+1)^2}{N^2R_0^2}\right) \sum_{q=0}^{2m-2} D_q \sum_{p=0}^{l+q} \frac{(l+q)!}{p!R_0^{2p}} \frac{(k+1)^{2p}}{N^{2p}} \\
 Q &= \frac{(l+m-1)!(3l+2m-1)}{(m-1)!} + 2l^2 \sum_{q=0}^{2m-2} D_q (q+l-1)! - 4l \sum_{q=0}^{2m-2} C_q (q+l)! \\
 C_q &= \sum_{p=\max(0,q-m+1)}^{\min(q,m-1)} b_p^{(l,m-1)} b_{q-p}^{(l+1,m-1)} \\
 D_q &= \sum_{p=\max(0,q-m+1)}^{\min(q,m-1)} b_p^{(l,m-1)} b_{q-p}^{(l,m-1)}
 \end{aligned}$$

where $R_0 = \rho_0/a$ is the equivalent (as a result of Gaussian approximation) normalized mode field radius (MFR); ρ_0 is the equivalent MFR; a is the MMF core radius; l is the azimuthal mode; m is the radial mode of LP_{lm} orders. $V = k_0 a n_{max} \sqrt{2\Delta}$ is the normalized frequency; $k_0 = 2\pi/\lambda$ is the wavenumber; λ is the operating wavelength; $b_p^{(l,m)}$ is the expansion factor of the Laguerre polynomial representation in the form of a finite power series [23,24]:

$$L_m^{(l)}(x) = \sum_{q=0}^m b_q^{(l,m)} x^q = \sum_{q=0}^m (-1)^q \frac{(l+m)!}{(l+q)!(m-q)!q!} x^q. \tag{6}$$

The characteristic equation of the equivalent MFR that has the generalized form according to the Gaussian approximation [22] is

$$\frac{\partial U^2}{\partial R_0} = 0,$$

and it also leads to the following analytical expression:

$$-Q + V^2 \left[S_0 + \sum_{k=0}^{N-1} h_k (S_1 - S_2) \right] = 0 \tag{7}$$

where

$$\begin{aligned}
 S_0 &= \exp\left(-\frac{1}{R_0^2}\right) \sum_{q=0}^{2m-2} D_q \sum_{p=0}^{l+q} \frac{(l+q)!}{p!R_0^{2p}} (1 - pR_0^2) \\
 S_1 &= \exp\left(-\frac{k^2}{N^2R_0^2}\right) \sum_{q=0}^{2m-2} D_q \sum_{p=0}^{l+q} \frac{(l+q)!}{p!R_0^{2p}} \frac{k^{2p}}{N^{2p}} \left(\frac{k^2}{N^2} - pR_0^2\right) \\
 S_2 &= \exp\left(-\frac{(k+1)^2}{N^2R_0^2}\right) \sum_{q=0}^{2m-2} D_q \sum_{p=0}^{l+q} \frac{(l+q)!}{p!R_0^{2p}} \frac{(k+1)^{2p}}{N^{2p}} \left(\frac{(k+1)^2}{N^2} - pR_0^2\right).
 \end{aligned}$$

Here, the normalized equivalent MFR R_0 is the result of the numerical solution of the characteristic Equation (7) after substitution of the researched optical fiber geometrical parameters and the particular azimuthal and radial orders of the analyzed mode. In EMGA (as well as in the “classical” Gaussian approximation), R_0 is a basic single variational parameter, which completely describes the mode dispersion characteristics. Following the substitution of R_0 to the variational expression expressed

in Equation (5), this permits the evaluation of the core mode parameter U , which relates with the propagation constant β by the following well-known ratio [17,20]:

$$\beta^2 = k_0^2 n_{\max}^2 - \frac{U^2}{a^2}. \tag{8}$$

The solution of the characteristic Equation (7) by taking into account the further substitution to Equation (5) and then to Equation (8) should satisfy the guided mode cut-off condition [1,17,20]:

$$k_0 n_N < \beta \leq k_0 n_{\max}. \tag{9}$$

We also propose considering the optical confinement factor P_{core} as the second criterion for the identification of the “ghost” solutions:

$$P_{co}^{(lm)} \geq 0.5. \tag{10}$$

The last one is also described by the following analytical expression earlier on, which is derived within the Gaussian approximation approach [20,21]:

$$P_{co}^{(lm)} = \frac{(m-1)!}{(l+m-1)!} \sum_{q=0}^{2m-2} D_q (l+q)! \left[1 - \exp\left(-\frac{1}{R_0^2}\right) \sum_{p=0}^{l+q} \frac{1}{p! R_0^{2p}} \right]. \tag{11}$$

The proposed EMGA provides low degrees of error, with a reduction of total computational time, especially for the calculations of higher-order mode parameters under low error, even during the analysis of large core optical fibers with complicated forms refractive index profiles, including real commercially available MMF graded-index profiles with refractive index fluctuations and technological defects. The results of EMGA verification by the rigorous mixed finite element method are represented by details in earlier published studies [25].

2.4. Mode Delay

The mode delay is inversely related to the propagation constant β [1,17,22],

$$t_d = \frac{1}{v_g} = -\frac{\lambda^2}{4\pi\beta c} \frac{\partial\beta^2}{\partial\lambda} = -\frac{\pi}{k_0^2\beta c} \frac{\partial\beta^2}{\partial\lambda}, \tag{12}$$

and, respectively, to the core mode parameter derivative $\partial U^2/\partial\lambda$ [21]:

$$\frac{\partial\beta^2}{\partial\lambda} = -\frac{2k_0^2 n_{\max}^2}{\lambda} + k_0^2 \frac{\partial n_{\max}^2}{\partial\lambda} - \frac{1}{a^2} \frac{\partial U^2}{\partial\lambda} \tag{13}$$

$$\begin{aligned} \frac{\partial U^2}{\partial\lambda} = & \frac{(m-1)!}{(l+m-1)!} \left\{ -\frac{2Q}{R_0^3} \frac{\partial R_0}{\partial\lambda} + \frac{\partial V^2}{\partial\lambda} \left[X_0 + \sum_{k=0}^{N-1} h_k (X_1 - X_2) \right] + 2V^2 X_0^{(1)} \frac{\partial R_0}{\partial\lambda} \right. \\ & \left. + V^2 \sum_{k=0}^{N-1} \frac{\partial h_k}{\partial\lambda} (X_1 - X_2) + 2V^2 \frac{\partial R_0}{\partial\lambda} \sum_{k=0}^{N-1} h_k (X_1^{(1)} - X_2^{(1)}) \right\} \end{aligned} \tag{14}$$

where

$$\begin{aligned} X_0^{(1)} &= \exp\left(-\frac{1}{R_0^2}\right) \sum_{q=0}^{2m-2} D_q \sum_{p=0}^{l+q} \frac{(l+q)!}{p! R_0^{2p+3}} (1 - pR_0^2) \\ X_1^{(1)} &= \exp\left(-\frac{k^2}{N^2 R_0^2}\right) \sum_{q=0}^{2m-2} D_q \sum_{p=0}^{l+q} \frac{(l+q)!}{p! R_0^{2p+3}} \frac{k^{2p}}{N^{2p}} \left(\frac{k^2}{N^2} - pR_0^2\right) \\ X_2^{(1)} &= \exp\left(-\frac{(k+1)^2}{N^2 R_0^2}\right) \sum_{q=0}^{2m-2} D_q \sum_{p=0}^{l+q} \frac{(l+q)!}{p! R_0^{2p+3}} \frac{(k+1)^{2p}}{N^{2p}} \left(\frac{(k+1)^2}{N^2} - pR_0^2\right), \end{aligned}$$

while the equivalent MFR derivative analytical expressions are also written as finite nested sums with the following form [21]:

$$\frac{\partial R_0}{\partial \lambda} = \frac{S_0 \frac{\partial V^2}{\partial \lambda} + \sum_{k=0}^{N-1} \left[(S_0 - S_1) \left(h_k \frac{\partial V^2}{\partial \lambda} + V^2 \frac{\partial h_k}{\partial \lambda} \right) \right]}{-2V^2 \cdot \left[S_0^{(1)} + \sum_{k=0}^{N-1} h_k \left(S_1^{(1)} - S_2^{(1)} \right) \right]} \tag{15}$$

where

$$S_0^{(1)} = \exp\left(-\frac{1}{R_0^2}\right) \sum_{q=0}^{2m-2} D_q \sum_{p=0}^{l+q} \frac{(l+q)!}{p! R_0^{2p+3}} \left[(1 - pR_0^2)^2 - pR_0^4 \right]$$

$$S_1^{(1)} = \exp\left(-\frac{k^2}{N^2 R_0^2}\right) \sum_{q=0}^{2m-2} D_q \sum_{p=0}^{l+q} \frac{(l+q)! k^{2p}}{p! N^{2p} R_0^{2p+3}} \left[\left(\frac{k^2}{N^2} - pR_0^2\right)^2 - pR_0^4 \right]$$

$$S_2^{(1)} = \exp\left(-\frac{(k+1)^2}{N^2 R_0^2}\right) \sum_{q=0}^{2m-2} D_q \sum_{p=0}^{l+q} \frac{(l+q)! (k+1)^{2p}}{p! N^{2p} R_0^{2p+3}} \left[\left(\frac{(k+1)^2}{N^2} - pR_0^2\right)^2 - pR_0^4 \right].$$

2.5. Mode of Chromatic Dispersion Parameter

The same technique is applied to derive the analytical expressions for the mode of the chromatic dispersion parameter D , which is related to the propagation constant β by the well-known formula [1,17,22]:

$$D = -\frac{\lambda}{2\pi c} \left(2 \frac{\partial \beta}{\partial \lambda} + \lambda \frac{\partial^2 \beta}{\partial \lambda^2} \right). \tag{16}$$

Therefore, by differentiating Equation (13), we shall obtain a second partial derivative of the square of the propagation constant:

$$\frac{\partial^2 \beta^2}{\partial \lambda^2} = k_0^2 \left(\frac{\partial^2 n_{max}^2}{\partial \lambda^2} + \frac{6n_{max}^2}{\lambda^2} - \frac{4}{\lambda} \frac{\partial n_{max}^2}{\partial \lambda} \right) - \frac{1}{a^2} \frac{\partial^2 U^2}{\partial \lambda^2}, \tag{17}$$

and the expression for chromatic dispersion parameter can be rewritten in the following form [21]:

$$D = -\frac{\pi}{k_0^2 \beta c} \left[\frac{2}{\lambda} \frac{\partial \beta^2}{\partial \lambda} + \frac{\partial^2 \beta^2}{\partial \lambda^2} - \frac{1}{2\beta^2} \left(\frac{\partial \beta^2}{\partial \lambda} \right)^2 \right]. \tag{18}$$

After differentiating Equations (14) and (15) with respect to wavelength, the desired second derivatives of the square core mode parameter U^2 and the normalized equivalent mode field radius R_0 will be obtained:

$$\begin{aligned} \frac{\partial^2 U^2}{\partial \lambda^2} = & \frac{(m-1)!}{(l+m-1)!} \left\{ \frac{2M}{R_0^3} \left[\frac{3}{R_0} \left(\frac{\partial R_0}{\partial \lambda} \right)^2 - \frac{\partial^2 R_0}{\partial \lambda^2} \right] + \sum_{k=0}^{N-1} (X_1 - X_2) \left(h_k \frac{\partial^2 V^2}{\partial \lambda^2} \right. \right. \\ & + 2 \frac{\partial h_k}{\partial \lambda} \frac{\partial V^2}{\partial \lambda} + V^2 \frac{\partial^2 h_k}{\partial \lambda^2} \left. \right) + 2 \sum_{k=0}^{N-1} \left(X_1^{(1)} - X_2^{(1)} \right) \left(2h_k \frac{\partial V^2}{\partial \lambda} \frac{\partial R_0}{\partial \lambda} + 2V^2 \frac{\partial h_k}{\partial \lambda} \frac{\partial R_0}{\partial \lambda} + V^2 h_k \frac{\partial^2 R_0}{\partial \lambda^2} \right) \\ & \left. + 4V^2 \left(\frac{\partial R_0}{\partial \lambda} \right)^2 \left[X_0^{(2)} + \sum_{k=0}^{N-1} h_k \left(X_1^{(2)} - X_2^{(2)} \right) \right] + X_0 \frac{\partial^2 V^2}{\partial \lambda^2} + 2X_0^{(1)} \left(2 \frac{\partial V^2}{\partial \lambda} \frac{\partial R_0}{\partial \lambda} + V^2 \frac{\partial^2 R_0}{\partial \lambda^2} \right) \right\} \end{aligned} \tag{19}$$

where

$$X_0^{(2)} = \exp\left(-\frac{1}{R_0^2}\right) \sum_{q=0}^{2m-2} D_q \sum_{p=0}^{l+q} \frac{(l+q)!}{p! R_0^{2p+6}} \left[(1 - pR_0^2)^2 + \frac{R_0^2}{2} (pR_0^2 - 3) \right]$$

$$X_1^{(2)} = \exp\left(-\frac{k^2}{N^2 R_0^2}\right) \sum_{q=0}^{2m-2} D_q \sum_{p=0}^{l+q} \frac{(l+q)!}{p! R_0^{2p+6}} \frac{k^{2p}}{N^{2p}} \left[\left(\frac{k^2}{N^2} - pR_0^2\right)^2 + \frac{R_0^2}{2} \left(pR_0^2 - \frac{3k^2}{N^2}\right) \right]$$

$$X_2^{(2)} = \exp\left(-\frac{(k+1)^2}{N^2 R_0^2}\right) \sum_{q=0}^{2m-2} D_q \sum_{p=0}^{l+q} \frac{(l+q)! (k+1)^{2p}}{p! R_0^{2p+6} N^{2p}} \left\{ \left[\frac{(k+1)^2}{N^2} - p R_0^2 \right]^2 + \frac{R_0^2}{2} \left[p R_0^2 - \frac{3(k+1)^2}{N^2} \right] \right\}$$

$$\frac{\partial X_0^{(1)}}{\partial \lambda} = 2 X_0^{(2)} \frac{\partial R_0}{\partial \lambda}$$

$$\frac{\partial X_1^{(1)}}{\partial \lambda} = 2 X_1^{(2)} \frac{\partial R_0}{\partial \lambda}$$

$$\frac{\partial X_2^{(1)}}{\partial \lambda} = 2 X_2^{(2)} \frac{\partial R_0}{\partial \lambda},$$

and

$$\begin{aligned} \frac{\partial^2 R_0}{\partial \lambda^2} = & - \left[V^2 S_0^{(1)} + \sum_{k=0}^{N-1} h_k (S_1^{(1)} - S_2^{(1)}) \right]^{-1} \left\{ 2 \frac{\partial R_0}{\partial \lambda} \sum_{k=0}^{N-1} (S_1^{(1)} - S_2^{(1)}) \left(V^2 \frac{\partial h_k}{\partial \lambda} + h_k \frac{\partial V^2}{\partial \lambda} \right) \right. \\ & + \sum_{k=0}^{N-1} (S_1 - S_2) \left(\frac{h_k}{2} \frac{\partial^2 V^2}{\partial \lambda^2} + \frac{\partial h_k}{\partial \lambda} \frac{\partial V^2}{\partial \lambda} + \frac{V^2}{2} \frac{\partial^2 h_k}{\partial \lambda^2} \right) + 2 V^2 \left(\frac{\partial R_0}{\partial \lambda} \right)^2 \left[S_0^{(2)} + \sum_{k=0}^{N-1} h_k (S_1^{(2)} - S_2^{(2)}) \right] \\ & \left. + \frac{S_0}{2} \frac{\partial^2 V^2}{\partial \lambda^2} + 2 S_0^{(1)} \frac{\partial R_0}{\partial \lambda} \frac{\partial V^2}{\partial \lambda} \right\} \end{aligned} \quad (20)$$

where

$$S_0^{(2)} = \exp\left(-\frac{1}{R_0^2}\right) \sum_{q=0}^{2m-2} D_q \sum_{p=0}^{l+q} \frac{(l+q)!}{p! R_0^{2p+6}} \left\{ (1 - p R_0^2)^3 + \frac{R_0^2}{2} [p R_0^4 (3p - 1) - 3] \right\}$$

$$S_1^{(2)} = \exp\left(-\frac{k^2}{N^2 R_0^2}\right) \sum_{q=0}^{2m-2} D_q \sum_{p=0}^{l+q} \frac{(l+q)! k^{2p}}{p! N^{2p} R_0^{2p+6}} \left\{ \left(\frac{k^2}{N^2} - p R_0^2 \right)^3 + \frac{R_0^2}{2} \left[p R_0^4 (3p - 1) - \frac{3k^4}{N^4} \right] \right\}$$

$$S_2^{(2)} = \exp\left(-\frac{(k+1)^2}{N^2 R_0^2}\right) \sum_{q=0}^{2m-2} D_q \sum_{p=0}^{l+q} \frac{(l+q)! (k+1)^{2p}}{p! N^{2p} R_0^{2p+6}} \left\{ \left(\frac{(k+1)^2}{N^2} - p R_0^2 \right)^3 + \frac{R_0^2}{2} \left[p R_0^4 (3p - 1) - \frac{3(k+1)^4}{N^4} \right] \right\}$$

$$\frac{\partial S_0^{(1)}}{\partial \lambda} = 2 S_0^{(2)} \frac{\partial R_0}{\partial \lambda}$$

$$\frac{\partial S_1^{(1)}}{\partial \lambda} = 2 S_1^{(2)} \frac{\partial R_0}{\partial \lambda}$$

$$\frac{\partial S_2^{(1)}}{\partial \lambda} = 2 S_2^{(2)} \frac{\partial R_0}{\partial \lambda}.$$

2.6. Material Dispersion and Refractive Index Profile Parameters

The well-known Sellmeier equation [1,17] is utilized to take into account the material dispersion:

$$n(\lambda) = \sqrt{1 + \sum_{i=1}^3 \frac{A_i \lambda^2}{\lambda^2 - B_i^2}} \quad (21)$$

where A_i and B_i are Sellmeier's coefficients (B_i is also denoted as the resonance wavelength), which has been empirically measured for GeO₂-SiO₂ glass [26,27] under several particular dopant concentrations. Here, we shall apply the method described in detail in the published work [28], to estimate the Sellmeier coefficients at the graded-index profile points.

A passage from the differentiation operator to its square is utilized analogously to the propagation of constant derivatives. This passage will greatly simplify the expressions for the first and second derivatives of the refractive index written via the Sellmeier equation:

$$\frac{\partial n}{\partial \lambda} = \frac{1}{2n} \frac{\partial n^2}{\partial \lambda}$$

$$\frac{\partial n^2}{\partial \lambda} = -2\lambda \sum_{i=1}^3 \frac{A_i B_i^2}{(\lambda^2 - B_i^2)^2}. \quad (22)$$

$$\frac{\partial^2 n}{\partial \lambda^2} = \frac{1}{2n} \left[\frac{\partial^2 n^2}{\partial \lambda^2} - \frac{1}{2n^2} \left(\frac{\partial n^2}{\partial \lambda} \right)^2 \right]$$

$$\frac{\partial^2 n^2}{\partial \lambda^2} = \sum_{i=1}^3 \frac{2A_i B_i^2 (B_i^2 + 3\lambda^2)}{(\lambda^2 - B_i^2)^3}. \quad (23)$$

Therefore, the first and second derivatives of the profile height parameter Δ can be expressed as follows:

$$\frac{\partial \Delta}{\partial \lambda} = \frac{1}{2n_{max}^2} \left[(1 - 2\Delta) \frac{\partial n_{max}^2}{\partial \lambda} - \frac{\partial n_N^2}{\partial \lambda} \right] \quad (24)$$

$$\frac{\partial^2 \Delta}{\partial \lambda^2} = \frac{1}{2n_{max}^2} \left[(1 - 2\Delta) \frac{\partial^2 n_{max}^2}{\partial \lambda^2} - \frac{\partial^2 n_N^2}{\partial \lambda^2} - 4 \frac{\partial \Delta}{\partial \lambda} \frac{\partial n_{max}^2}{\partial \lambda} \right], \quad (25)$$

while derivatives of the local profile parameter h_k lead to the following expressions:

$$\frac{\partial h_k}{\partial \lambda} = \frac{1}{n_{max}^2 - n_N^2} \left[(1 - h_k) \frac{\partial n_{max}^2}{\partial \lambda} - \frac{\partial n_k^2}{\partial \lambda} + h_k \frac{\partial n_N^2}{\partial \lambda} \right] \quad (26)$$

$$\frac{\partial^2 h_k}{\partial \lambda^2} = \frac{1}{n_{max}^2 - n_N^2} \left[(1 - h_k) \frac{\partial^2 n_{max}^2}{\partial \lambda^2} - \frac{\partial^2 n_k^2}{\partial \lambda^2} + h_k \frac{\partial^2 n_N^2}{\partial \lambda^2} - 2 \frac{\partial h_k}{\partial \lambda} \left(\frac{\partial n_{max}^2}{\partial \lambda} - \frac{\partial n_N^2}{\partial \lambda} \right) \right]. \quad (27)$$

Finally, by applying Equations (22) and (23), the first and second derivatives of the normalized frequency V can be expressed by the following formulas:

$$\frac{\partial V^2}{\partial \lambda} = a^2 k_0^2 \left[\frac{\partial n_{max}^2}{\partial \lambda} - \frac{\partial n_N^2}{\partial \lambda} - \frac{2}{\lambda} (n_{max}^2 - n_N^2) \right] \quad (28)$$

$$\frac{\partial^2 V^2}{\partial \lambda^2} = -\frac{2}{\lambda} \frac{\partial V^2}{\partial \lambda} + a^2 k_0^2 \left\{ \frac{\partial^2 n_{max}^2}{\partial \lambda^2} - \frac{\partial^2 n_N^2}{\partial \lambda^2} + \frac{2}{\lambda} \left[\frac{1}{\lambda} (n_{max}^2 - n_N^2) - \frac{\partial n_{max}^2}{\partial \lambda} + \frac{\partial n_N^2}{\partial \lambda} \right] \right\}. \quad (29)$$

2.7. Model of a Piecewise Regular Multimode Fiber Optic Link Operating in a Few-Mode Regime under Laser-Excited Optical Pulse Propagation

We propose utilizing a previously developed model of a piecewise regular multimode fiber optic link operating in a few-mode regime to simulate laser-excited optical pulse propagation, and to estimate the potentiality of a 100 μm core MMF, as well as an optimized 100 μm core LDMDF for laser-based multi-gigabit data transmission. This model is described in detail in the published work [21], where its experimental verification is also demonstrated. The proposed solution is based on piecewise regular representation, combined with the general approach of the split-step method [29] to simulate the processes of mode mixing and power diffusion occurring due to mode coupling (Figure 1). Here, single silica weakly guiding circular MMF with an arbitrary axially symmetric refractive index profile with single continuous outer cladding is considered. According to the piecewise regular representation, the fiber is divided into regular spans with length Δz . Inside of the span, the fiber geometry parameters are considered as a constant, and the modes propagate independently without interaction and mixing. It is supposed that each excited guided mode with a propagation constant, varying from one regular span to another span, satisfies a cut-off condition for whole regular spans composing the fiber. Additionally, it is assumed that at the link transmitter end, each excited guided mode begins transferring a single optical pulse with a particular form that is identical to the input signal (for example, Gaussian). During pulse propagation over a regular span, its amplitude decreases, due to mode attenuation. The signal

is mainly distorted due to the difference between the group velocities and the amplitudes of modes, i.e., the DMD effect. Additionally, the transfer by the pulse spreading of each mode due to chromatic dispersion for a particular mode is taken into account.

The boundaries of regular spans can be represented generally as ideal axial alignment splices of two almost similar optical fibers with mismatching parameters. However, it is correct only for “straight” fibers. Therefore, we propose simulating fiber bends by the representation of boundaries in the form of splices of two mismatched fibers with some low angular misalignment [21]. The mode power redistribution between the amplitudes of signal components as a result of mode interaction is estimated by mode coupling of coefficient matrix computing at the joints of regular spans. Here, only guided modes are considered as the main issue under pulse dynamics research during the propagation over a multimode fiber link in a few-mode regime. However, power loss due to component transformation from guided to leaky mode and reflections are also indirectly taken into account.

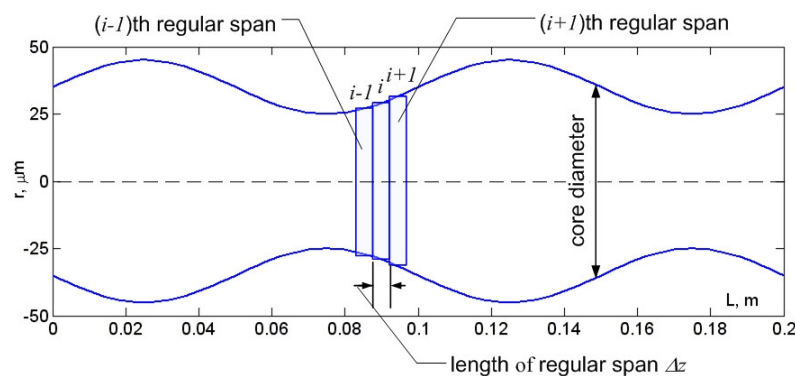


Figure 1. Piecewise regular representation of 200 m of irregular optical fiber with varying core diameters.

At the receiver end, the resulting pulse envelope is considered as a superposition of all mode components of the signal. Here, it is proposed that a well-known expression is applied for the frequency response of the signal transferred by the M mode components LP_{lm} over a regular multimode fiber with length z [1]:

$$H_{Rxt}(\omega, z) = F[h_{Tx}(t)] \sum_p^M A_p^{(0)} \exp(-\alpha_p z) \exp[-j(\omega - \omega_0)\beta_1^{(p)} z] \exp\left[-j\frac{1}{2}(\omega - \omega_0)^2 \beta_2^{(p)} z\right] \quad (30)$$

where F is the direct Fourier transform; $h_{Tx}(t)$ is the initial pulse at the transmitter end; $A_p^{(0)}$ and α_p are the starting amplitude and the mode attenuation of the p -th guided mode LP_{lm} ($p = 1..M$); $\beta_1^{(p)}$ and $\beta_2^{(p)}$ are first- and second-order dispersion parameters. These dispersion parameters are elements of the well-known Taylor series expansion approximation of the propagation constant frequency dependence $\beta(\omega)$ [1,17,29]:

$$\beta(\omega) = (\omega - \omega_0)\beta_1 + \frac{1}{2}(\omega - \omega_0)^2 \beta_2 + \frac{1}{6}(\omega - \omega_0)^3 \beta_3 \dots$$

where

$$\beta_n = \left[\frac{\partial^n \beta}{\partial \omega^n} \right]_{\omega=\omega_0}.$$

Here, $\beta_1^{(p)} = \tau^{(p)}$ is the mode delay and $\beta_2^{(p)}$ is the group velocity dispersion associated with the chromatic dispersion of the p -th guided mode, LP_{lm} .

Therefore, according to introduced piecewise regular representation of the irregular multimode fiber link, the frequency response of a few-mode optical signal, transferred by M guided modes over an irregular MMF with length z under a given particular length of regular span Δz by taking Equation (30) into account, can be written in the following form [21]:

$$\begin{aligned}
 H_{Rx}(\omega, z) = & F[h_{Tx}(t)] \sum_p^M A_{(N_z+1)}^{(p)} \exp\left[-\alpha_{(N_z+1)}^{(p)}(z - N_z \Delta z)\right] \exp\left[-j(\omega - \omega_0)\tau^{(p;N_z+1)}(z - N_z \Delta z)\right] \\
 & \times \exp\left[-j\frac{1}{2}(\omega - \omega_0)^2 \beta_2^{(p;N_z+1)}(z - N_z \Delta z)\right] \prod_{q=1}^{N_z} A_q^{(p)} \exp\left(-\alpha_q^{(p)} \Delta z\right) \\
 & \times \exp\left(-j(\omega - \omega_0)\tau^{(p;q)} \Delta z\right) \exp\left(-j\frac{1}{2}(\omega - \omega_0)^2 \beta_2^{(p;q)} \Delta z\right)
 \end{aligned} \tag{31}$$

where $N_z = E(z/\Delta z)$; $E(x)$ is the integer part of the real number x .

The resulting pulse response at the receiver end of the irregular multimode link is computed by the following simple expression:

$$h_{Rx}(t) = F^{-1}(H_{Rx}(\omega)) \cdot \left[F^{-1}(H_{Rx}(\omega)) \right]^* \tag{32}$$

where F^{-1} is the inverse Fourier transform; $[x]^*$ is the complex conjugate of x .

Therefore, EMGA is applied for computing the dispersion parameters of the desired selected order guided modes at each regular span of the researched irregular MMF, including mode delays (or group velocity) and chromatic dispersion parameters. Differential mode attenuation is estimated by the known empirical expression proposed by Yabre in [30], which is based on experimental data represented by the same author in [31]:

$$\alpha_\mu(\lambda) = \alpha_0(\lambda) + \alpha_0(\lambda) I_9 \left[7.35 \left(\frac{\mu - 1}{M_0} \right)^{\frac{2g}{g+2}} \right] \tag{33}$$

where $\mu = 2m + l + 1$ is principal mode number; $\alpha_0(\lambda)$ is the attenuation of lower-order modes (it is supposed to be equal to the attenuation at the correspondence wavelength mentioned in fiber specification); M_0 is total number of modes satisfying the cutoff condition for the analyzed fiber:

$$M_0(\lambda) = 2\pi \frac{n_{\max}(\lambda)}{\lambda} \sqrt{\frac{g\Delta(\lambda)}{g+2}}$$

where g is the gradient factor of the smoothed α -profile.

The model presented passed experimental approbation: a good agreement between its simulation and direct experimental measurements of pulse response was obtained, which was described in detail in the published work [21].

2.8. Mode Coupling

Research on the irregularity of MMF is concerned with core diameter variations. Therefore, we propose setting it directly via an array from the reports of optical fiber diameter measurements that were produced during fiber drawing. Micro- and macro-bends are simulated by random equivalent low ($\theta = 2.0^\circ \dots 4.0^\circ$) angular misalignments [21] at the boundaries of regular spans, while mode coupling coefficient redistribution at the span boundaries as well as at the optical interconnections of the transmitter and receiver ends may be estimated by the well-known mode field overlap integral method [1,17,22], taking into account the particular angular misalignment inserted. Here, we utilized the overlap integral method in combination with the introduced EMGA, which takes into account the local features of the real silica optical fiber refractive index profile and decreases the computational error. A passage from the generalized form of the overlap, integral to the analytical expression for the arbitrary order mode coupling coefficient estimation at the centralized splice of the optical fibers with mismatched parameters without any misalignments, was proposed in [32]. The analytical expression derivation is described in detail in [33]. Finally, the formula for the arbitrary order mode coupling coefficient at the central splice is written as follows:

$$\eta_{mn} = \frac{\Gamma(m)\Gamma(n)}{\Gamma(l+m)\Gamma(l+n)} (2\rho_m\rho_n)^{2l+2} \left[\frac{(\rho_m - \rho_n)^{m+n-2}}{(\rho_m^2 + \rho_n^2)^{m+n+l-1}} \right]^2 \times \left\{ \sum_{k=0}^{\min\left(\frac{n-1}{m-1}\right)} (-1)^k \frac{\Gamma(m+n+l-k-1)}{\Gamma(m-k)\Gamma(n-k)k!} \left(\frac{\rho_m^2 + \rho_n^2}{\rho_m - \rho_n} \right)^k \right\} \tag{34}$$

where mode coupling occurs only for modes with the same azimuthal order l ; Γ is the gamma function; ρ_m and ρ_n are the injected LP_{lm} and excited LP_{ln} mode field radiuses, respectively.

The analytical expression for the arbitrary order mode coupling coefficient at the optical fiber splice under a low angle misalignment $\theta < 10^\circ$ derived and represented in [33] has the following form:

$$\eta_{mn}^{(\theta)} = 4 \frac{(m-1)!}{(l_m+m-1)!} \frac{(n-1)!}{(l_n+n-1)!} \left\{ \sum_{p=0}^{m+n-2} \sum_{q=\max(0,p-n+1)}^{\min(p,m-1)} b_q^{(l_m,m-1)} b_{p-q}^{(l_n,n-1)} \frac{2^{\frac{lp}{2}+p} (k_0 n_\theta \theta)^{lp} \Gamma(\frac{lp}{2} + l_n + p + 1)}{(\rho_m^2 + \rho_n^2)^{\frac{lp}{2} + l_n + p + 1} (l_n)!} \times \rho_m^{2(l_n+p-q)+1} \rho_n^{l_m+l_n+2q+1} \cdot {}_1F_1 \left[\left(\frac{l_m}{2} + l_n + p + 1 \right), (l_n + 1); -(k_0 n_\theta \theta)^2 \frac{\rho_m^2 \rho_n^2}{(\rho_m^2 + \rho_n^2)} \right] \right\}^2 \tag{35}$$

where ${}_1F_1$ is the confluent hypergeometric function of the first kind [23,24]:

$${}_1F_1(a, b; x) = 1 + \sum_{p=1}^{\infty} \left[\prod_{q=0}^{p-1} \frac{(a+q)x}{(1+q)(b+q)} \right]$$

where $b_q^{(l_m,m-1)}$ and $b_q^{(l_n,n-1)}$ are Laguerre polynomial expansion factors of Equation (6); n_θ is the refractive index of the launching medium (air gap, core of adjusting/exiting fiber, etc.).

3. Results

3.1. Low Differential Mode Delay Fiber with a Large 100 μm Core Diameter

In the first step, we utilized a LOMF 50/125 refractive index profile scaled to a 100 μm core diameter as the reference for further computation of the selected guided mode staff DMD diagram, to define the boundaries of the reference mode delay t_{REF} range. The reference graded refractive index profile was set by a data protocol of measurements, performed by a certified optical fiber analyzer for a sample of a commercially available LOMF of ISO/IEC Cat. OM2+/OM3 [34], and scaled up to a 100 μm core. This is represented in Figure 2.

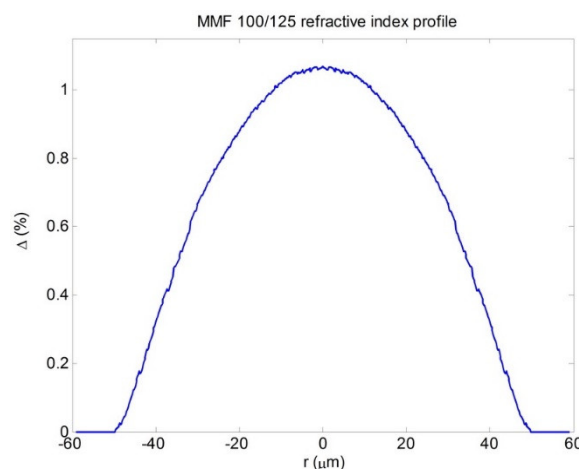


Figure 2. Reference graded refractive index profile reconstructed by a report of real laser-optimized multimode fiber (LOMF) sample profile measurements and scaled up to a 100 μm core.

This profile is quite smooth, and it may be considered as an almost graded power law profile. However, it is not a pure α -profile, and it differs from the last one by the “non-power-law” envelope and by weak local fluctuations of the refractive index improving close to the fiber core center area. By using EMGA, we performed an analysis of a reference 100 μm core MMF with a refractive index over the “O”-band. According to the computational results, it supports the propagation of 145 modes LP_{lm} ($l = 0, \dots, 24; m = 1, \dots, 11$) satisfying the cutoff conditions with an optical confinement factor $P_{co} > 0.5$, whose distribution over the total mode staff at wavelength $\lambda = 1310$ nm is shown in Figure 3.

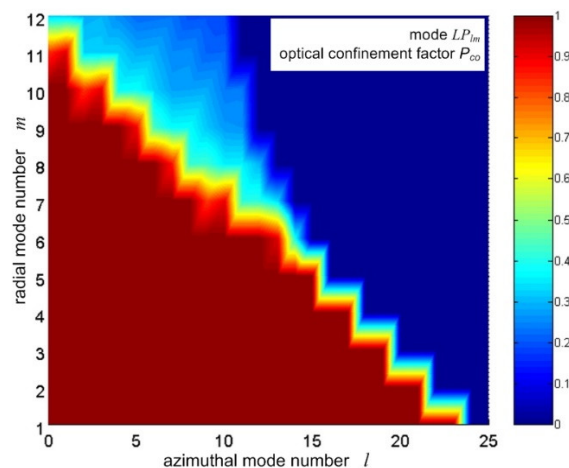


Figure 3. Optical confinement factor distribution over the mode staff of a reference 100 μm core multimode optical fiber (MMF).

During the design, with an MMF with an improved bandwidth under a multimode regime, all guided mode staff delays should be equalized, while according to the presented method, only guided modes with normalized amplitudes of more than 0.1 should be considered under particular launching conditions. Here, we propose the centralized launching of the optical signal generated by conventional Fabry–Perot laser diode-generating emission at $\lambda = 1310$ nm to the MMF core end via a standard single mode optical fiber (ITU-T Recommendations G.652), which in the “worst case” may support the propagation of two modes, LP_{01} and LP_{11} , at the mentioned wavelength. According to the model described above for the simulation of a piece-wise regular multimode fiber optic link operating in a few-mode regime, mode mixing and power diffusion due to micro- and macro-bends are simulated as connections of the researched MMF regular spans performed with weak angular misalignment ϕ . This supposition was confirmed by experimental verification of the model [21], while it was found that for MMF coiled on a typical fiber spool, this angular misalignment can vary as much as $\phi = 2.0\text{--}3.5^\circ$. Therefore, we performed the computation of normalized amplitude distribution dynamics over a guided mode staff under centralized mode LP_{01} and LP_{11} launching conditions, and further mode power redistribution due to bends for 11 regular spans of piece-wise regular representation. The results of the mode staff normalized amplitude dynamics calculation are shown in Figure 4. Here, we noticed that only 21 guided modes LP_{lm} ($l = 0, \dots, 7; m = 1, \dots, 5$) transfer the majority of the optical signal during its propagation over the reference 100 μm core MMF, and that their delays vary from 4.922 up to 4.924 ns/km, defining the range for the reference value t_{REF} setting, while normalized amplitudes of other components are less than 0.1.

We performed the synthesis of LDMDF 100/125 desired refractive index profiles for various combinations of t_{BASE} and α -parameters of a first iteration graded profile. The result of 100 μm core LDMDF refractive index profile optimization under $t_{REF} = 4923.08$ ns/km and $\alpha = 1.900$ for centralized launching conditions is shown in Figure 5, while a comparison between the DMD diagrams for the reference MMF and a sample of LDMDF is shown in Figure 6.

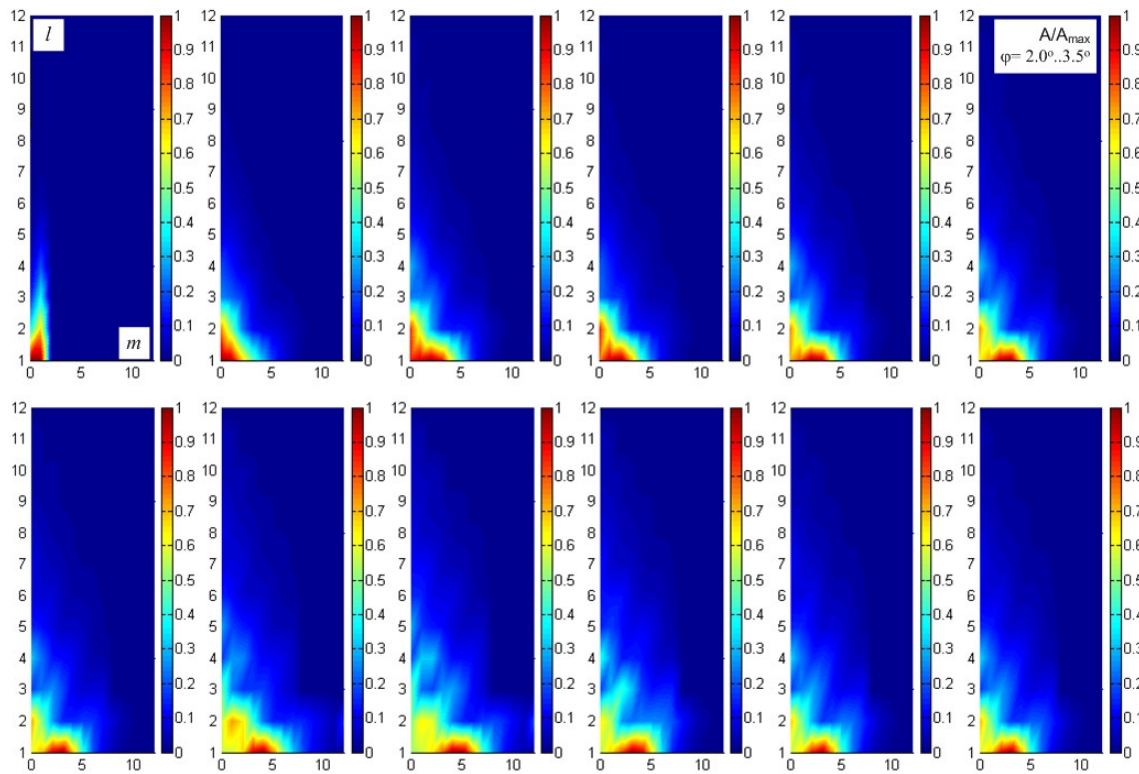


Figure 4. Normalized amplitude distribution dynamics over the guided mode staff of the reference MMF under a centralized mode LP_{01} and LP_{11} launching, and following mode mixing and power redistribution due to the fiber bends being represented as a connection of regular spans with weak angular misalignment, which is empirically defined as a range of $\phi = 2.0^\circ \dots 3.5^\circ$.

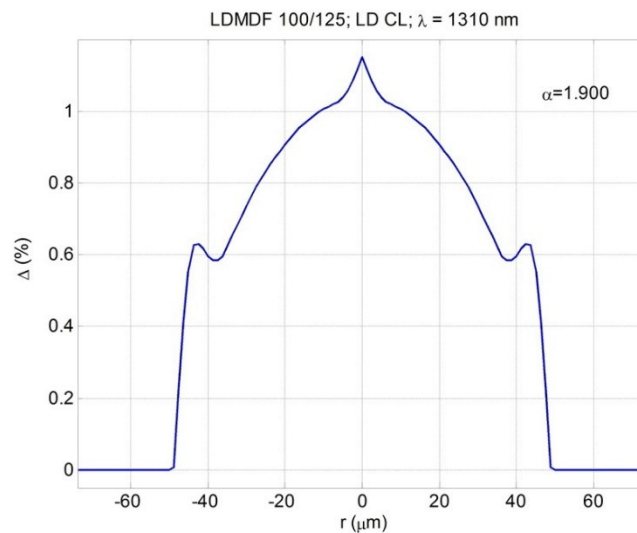


Figure 5. Optimized graded refractive index profile for a 100 μm core low differential mode delay fiber (LD MDF).

Spectral curves of DMD regarding to the fundamental mode $DMD_{LP_{01}}(\lambda)$ computed over the “O”-band for both the reference 100 μm core MMF and LD MDF samples are represented in Figure 7: (a) corresponds to the total “O” band, while (b) shows the LD MDF and DMD curve fragment over a $\lambda = 1310 \text{ nm}$ wavelength region. For the reference MMF, DMD varies from 1589.7 ps/km up to 1950.5 ps/km over the “O”-band, while the optimized refractive index profile provides a decrease of DMD from 5.0–6.0 times at the boundaries of the “O”-band, and up to 9.0 and more times at a $\lambda = 1310 \text{ nm}$ region in comparison with the reference MMF. Here, the total value of $DMD_{LP_{01}}$ is not

more than 300 ps/km over all of the “O”-band; the lowest DMD_{LP01} is 176.2 ps/km, and it corresponds to 1285 nm; for $\lambda = 1310$ nm, $DMD_{LP01} = 255.7$ ps/km.

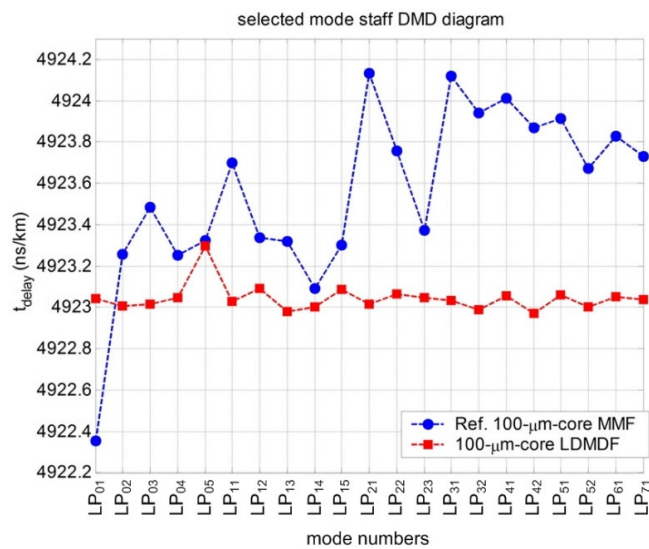


Figure 6. DMD diagrams computed for selection under a centralized launching condition mode staff for the reference MMF and LDMDF.

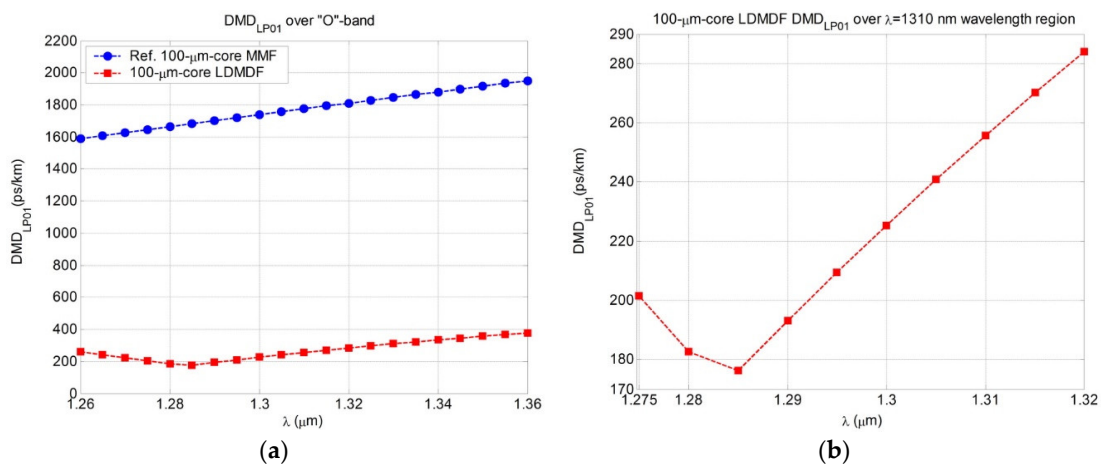


Figure 7. Spectral DMD (λ) curves over the “O”-band: (a) the reference MMF and the LDMDF samples; (b) the $\lambda = 1310$ nm wavelength region.

3.2. Simulation of 10GBase-LX Fiber Optic System Optical Pulse Propagation

In the first step, we simulated a 10GBase-LX fiber optic system optical pulse propagation over a 100 μm core MMF with a total length of 2 km, and described the above refractive index profile presented in Figure 2, which corresponds to the measured real commercially available sample of the LOMF ISO/IEC 11801 OM2+/OM3 Cat. (MMF 50/125) profile [34], which was scaled up to a 100 μm core region. According to the previous paragraph results, this MMF provides the DMD with about 1800 ps/km at an operating wavelength of the 10GBase-LX system— $\lambda = 1310$ nm.

Fiber irregularity is considered as the core diameter variations that are assigned by the array, taken from reports of commercially available MMF 50/125 outer diameter measurements performed during fiber drawing [35] under a mean deviation of ± 0.271 μm from the average value of 125.022 μm . Its fragment of over 2 km in length regarding the reference value of the core radius and statistics are shown in Figure 8. The length of a regular span is set to be equal to the fiber diameter measurement workstation spatial resolution, $\Delta z = 8$ m. Micro- and macro-bends of the researched fiber are simulated by random equivalent low angular misalignments [21] at the boundaries of regular spans. We consider

a “stressed and bended” MMF that is simulated by normal distribution under a mean of 3.0° and a deviation of 0.5° . Its distribution over 2 km of MMF length and its statistics are presented in Figure 9.

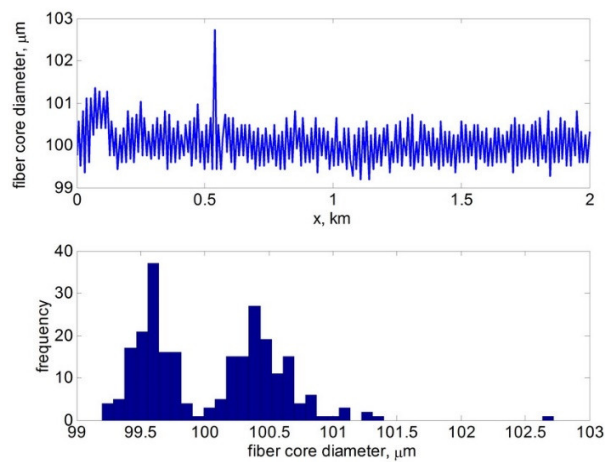


Figure 8. Variation of the core diameter along the researched optical fiber length.

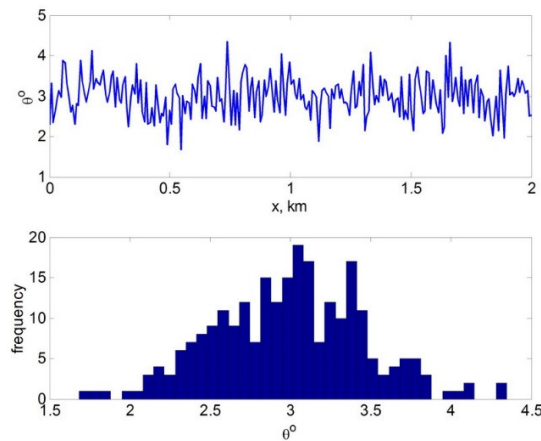


Figure 9. Variation of the equivalent angular misalignment at the splice of regular spans along the fiber length simulating fiber micro- and macro-bends.

We simulated the propagation of a Gaussian-shaped optical pulse with a full width of half maximum FWHM = 90.91 ps that corresponds to a 10 Gbps bit rate excited by laser diodes operating at a wavelength $\lambda = 1310$ nm, generating two LP-mode (linear polarized mode) optical emissions containing the fundamental LP_{01} and the higher-order mode LP_{11} . Here, the “worst case” of launching conditions was considered, which corresponds to a connection via a conventional fiber optic adapter simulated as a connection with an angular misalignment $\theta = 4.20^\circ$ [36] between a standard single-mode optical fiber (ITU-T Recommendations G.652) of a laser source pigtail and a link 100 μm core MMF.

The results of the simulation of 10GBase-LX optical pulse dynamics during propagation over a 100 μm core MMF with a total length of 2 km without special launching conditions is represented in Figure 10a,b (pulse dynamics and diagram of pulse propagation). It was unexpected, but the optical signal kept its envelope without strong DMD distortions, up to a distance of almost 0.45 km from the transmitter end, even without special launching conditions, which is quite sufficient for on-board cable system fiber optic links that are characterized by extremely short ranges. However, further strong DMD occurred with increasing distance.

In the second step, we researched the potentiality of the designed 100 μm core LDMDF sample potentiality for laser-based 10 Gbps data transmission under the same “the worst case” launching conditions, and variations of both the core diameter and the equivalent angular misalignment at the boundaries of the regular spans. The results of the simulation of 10GBase-LX optical pulse

dynamics during propagation over a 100 μm core LDMDF with a total length of 2 km without special launching conditions is represented in Figure 11. The LDMDF sample shows a great potentiality for applications in multi-gigabit network fiber optic links: here, DMD distortions did not occur over the entire monitored 2 km length.

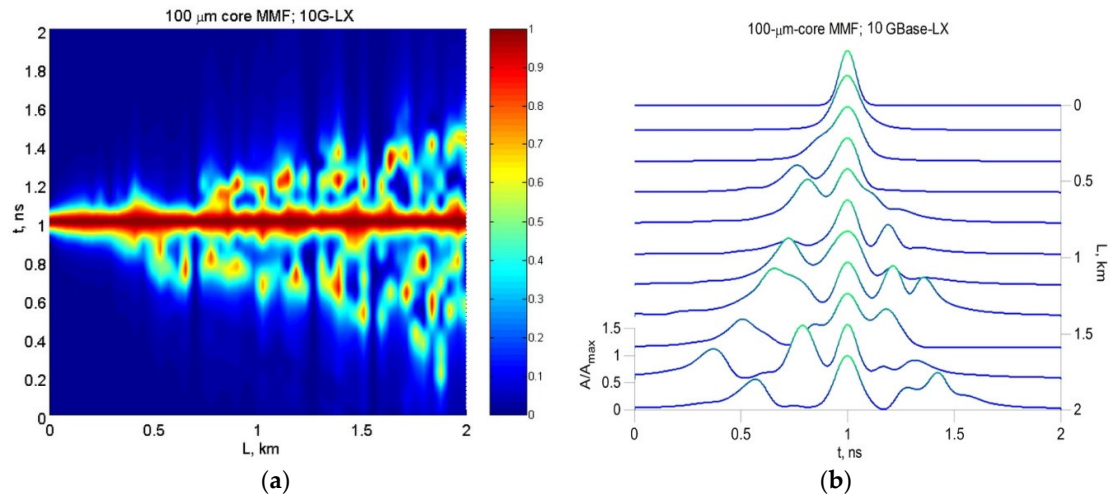


Figure 10. 10GBase-LX optical pulse dynamics during propagation over a 100 μm core MMF with a total length of 2 km without special launching conditions: (a) pulse dynamics; (b) diagram of pulse propagation.

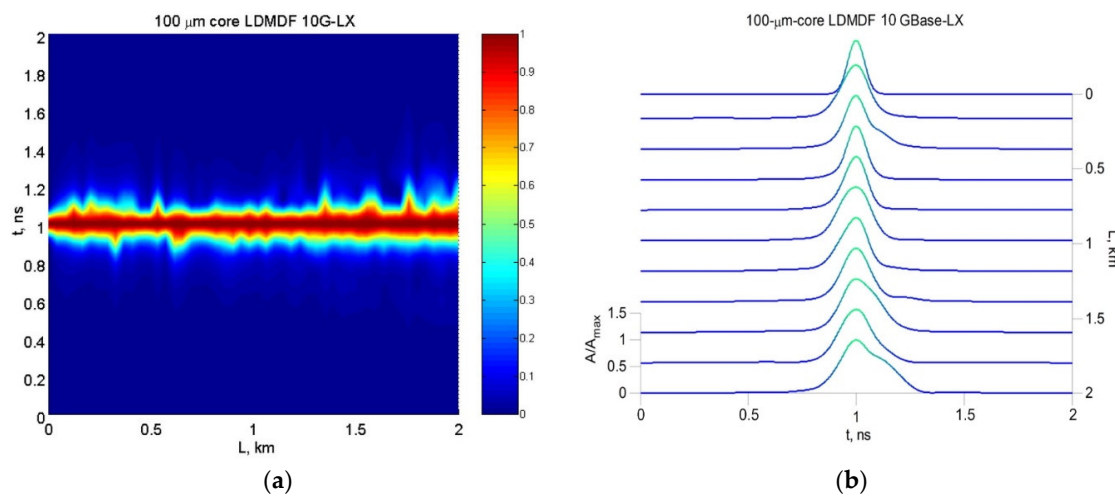


Figure 11. 10GBase-LX optical pulse dynamics during propagation over a 100 μm core LDMDF with a total length of 2 km without special launching conditions: (a) pulse dynamics; (b) diagram of pulse propagation.

4. Discussion

The results of optical signal propagation simulation over a 100 μm core MMF and LDMDF with a length of 2 km presented in the previous section allow for the localization of a maximal distance where the optical pulse keeps its envelope, and where a strong DMD “glove” effect does not arise, while estimation of the fiber optic system channel quality requires the evaluation of the bit error ratio (BER) or the Q-factor, by taking into account the dispersion distortions. Therefore, we propose computing the optical signal dispersion at the receiver end under a particular distance by a known method for the processing of pulses with arbitrary forms, as described in detail in the monograph [37], and other issues, while, for the first time, the estimation of the 10GBase-LX channel Q-factor, performed by using “the worst case” link model developed by the IEEE 802.3z Task Force, declared and ratified the ability for laser-based data transmission to proceed over MMFs with a 1 Gbps bit rate [38,39].

By analyzing the computation results of pulse dynamics according to the above-mentioned method, we found that pulse dispersion at the receiver end under a maximal 0.45 km length of the 100 μm core MMF, providing a negligible DMD effect, is $D = 83.583$ ps. The pulse response is shown in Figure 12a. During the next step, we performed an estimation of the Q-factor for the conventional 9.2 dB budget 10GBase-LX transceiver, by taking into account the pulse dispersion, as well as other distortion factors/penalties according to the model [38,39]. The computed eye-diagram envelope is represented in Figure 12b: Here, the Q-factor is 4.968, which is unacceptably lower in comparison with the reference value $Q_{REF} = 7.04$, which corresponds to the “worst case” BER = 10^{-12} required by a 10GBase-LX specification without a forward error correction (FEC) technique [40]. As a result, a maximal 100 μm core MMF length $L = 0.286$ km was localized: here, the total pulse dispersion is $D = 62.329$ ps (Figure 12a), which provides a desired Q-factor of 8.236 (Figure 12b).

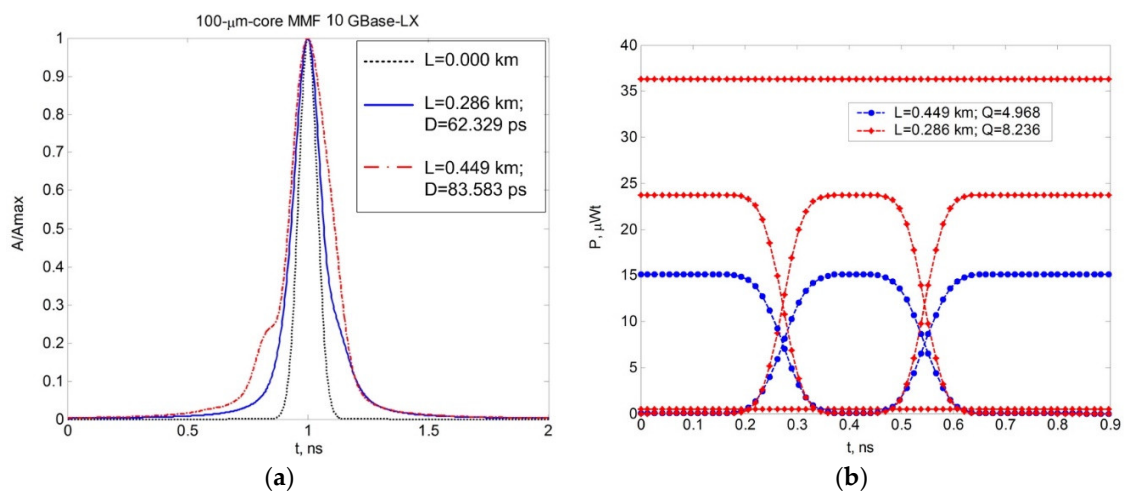


Figure 12. 10GBase-LX data transmission over a 100 μm core MMF without special launching conditions: (a) pulse response; (b) eye diagram envelope.

Regarding the 100 μm core LDMDF, the optical pulse maintains its envelope over the total fiber length of 2 km, and its dispersion at the receiver end is $D = 92.113$ ps. As expected, this is an unacceptably high value that leads to a low Q-factor of 3.656. For this reason, we also localized the maximal distance for a 100 μm core LDMDF link that provides the required 10GBase-LX specification Q-factor value: here, it is $L = 1.020$ km with a pulse dispersion $D = 43.669$ ps and $Q = 8.660$ (Figure 13a,b).

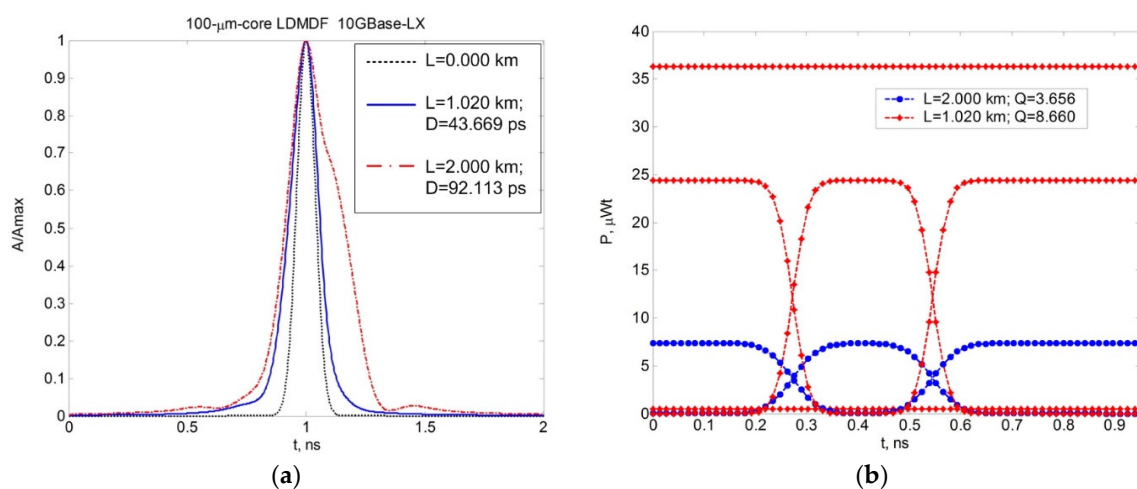


Figure 13. 10GBase-LX data transmission over a 100 μm core LDMDF without special launching conditions: (a) pulse response; (b) eye diagram envelope.

5. Conclusions

We here present an alternative fast and simple method for a design refractive index profile of silica LDMDFs with an extremely enlarged core diameter of up to 100 μm , for laser-based multi-gigabit short-range optical networks. The results of the 100 μm core LDMDF graded index profile sample optimization performed by the proposed solution, and the following computation of the DMD spectral curve over the “O”-band, were demonstrated and compared with a “reference” 100 μm core MMF, where the refractive index profile is similar to the conventional commercially available LOMF, scaled up to a 100 μm core. For the reference MMF, DMD varies from 1589.7 ps/km up to 1950.5 ps/km over the above-mentioned wavelength band. The optimized refractive index profile provides a decreasing of DMD from 5.0–6.0 times at the boundaries of the “O”-band, up to 9.0 and more times at the $\lambda = 1310$ nm region, in comparison with the reference MMF. Here, the DMD is not more than 300 ps/km over the entire “O”-band, while the least $DMD_{LP01} = 176.2$ ps/km, and it corresponds to 1285 nm, and $DMD_{LP01} = 255.7$ ps/km at $\lambda = 1310$ nm. We utilized a previously developed alternative method for the simulation of piecewise regular multimode fiber optic links operating in a few-mode regime for the computation of laser-excited 10GBase-LX optical pulse dynamics during its propagation over irregular 100 μm core optical fibers—the reference MMF and the optimized LDMDF. While most of the commercially available MMFs with a 100 μm core diameter are targeted to only multimode regimes, and the utilized transceivers based on multimode LEDs provide low bit rates of 10–100 Mbps of data transmission, our simulation results demonstrate the implementation of 10GBase-LX channels over both short-length MMFs with a LOMF-graded refractive index profile, and scaled up to a 100 μm core and extended distance links provided by LDMDFs with an optimized graded refractive index profile. Here, in spite of uncontrolled launching conditions corresponding to connection via a conventional fiber optic adapter simulated as a connection with an angular misalignment $\theta = 4.20^\circ$ between a standard single-mode optical fiber (ITU-T Recommendations G.652) of a laser source pigtail and a link optical fiber, even the 100 μm core MMF keeps a pulse envelope for a distance of up to 0.5 km, with a total dispersion of about 85 ps, while LDMDF blocks up the DMD over the entire 2 km length with a total pulse dispersion of not more than $D = 32$ ps under a length $L = 0.5$ km, and $D = 92.50$ ps under a length $L = 2.0$ km. According to “the worst case link model” developed by the IEEE 802.3z Task Force, we estimate the Q-factor for the 10GBase-LX channel based on 9.2 dB budget IEEE 802.3ae LX-transceivers and a 100 μm core reference MMF and LDMDF without any special launching conditions under a particular fiber length. As a result, the maximal lengths of both MMF and LDMDF were localized to provide the least reference $Q = 7.04$ for $BER = 10^{-12}$: for a 100 μm core MMF, this distance was $L = 0.286$ km under a total pulse dispersion $D = 62.329$ ps and $Q = 8.236$; for the 100 μm core LDMDF with a designed special refractive index profile, even under the length $L = 1.020$ km, the Q-factor is a desirable reference value ($Q = 8.660$) under a total pulse dispersion of $D = 43.669$ ps.

Author Contributions: Core idea and conceptualization: A.V.B. and V.A.B.; methodology: A.V.B., V.A.B., V.J., and G.S.; design and simulations: A.V.B. and A.E.Z.; verification: A.V.B., A.E.Z., and A.K.G.; investigation: A.V.B., A.E.Z., and A.K.G.; data curation: A.V.B., V.A.B., V.J., and G.S.; writing—original draft preparation, A.V.B. and A.E.Z.; writing—review and editing, A.V.B., V.A.B., V.J., and G.S.; visualization—A.E.Z.; supervision—A.V.B.; all authors discussed the results and contributed to the final manuscript.

Funding: This research was funded RFBR, Grant No. 16-37-60015 mol_a_dk.

Acknowledgments: The authors would like to thank Egishe V. Ter-Nersesyants, and Vladimir V. Demidov (Research and Technological Institute of Optical Materials, All-Russia Scientific Center “S.I. Vavilov State Optical Institute”, St. Petersburg, Russia) for providing reports of the optical fiber outer diameter measurements during the drawing process.

Conflicts of Interest: The authors declare no conflict of interest.

References

1. Bottacchi, S. *Multi-Gigabit Transmission over Multimode Optical Fibre: Theory and Design Methods for 10GbE Systems*; John Wiley & Sons Ltd.: New York, NY, USA, 2008; ISBN 13 978-0-471-89175-8.
2. Kamino, J. It's Time for OM5! BICSI Presentation Materials 2017. Available online: https://www.bicsi.org/uploadedfiles/bicsi_conferences/fall/2017/presentations/CONCSES_1C.pdf (accessed on 31 August 2018).
3. Mazzaresse, D. Optical fiber choice for data centers. *Commun. Technol. Equip.* **2009**, *4*, 30–32.
4. Irujo, T. OM4 Fiber—The Next Generation of Multimode Fiber. BICSI Presentation Materials 2017. Available online: <http://www.bicsi.org/pdf/presentations/canada2010/OM4%20Multimode%20Fibers.pdf> (accessed on 31 August 2018).
5. Freund, R.E.; Bunge, C.-A.; Ledentsov, N.N.; Molin, D.; Caspar, C. High-speed transmission in multimode fibers. *IEEE J. Lightwave Technol.* **2010**, *28*, 569–586. [CrossRef]
6. Roberts, C.; Ellis, R. *Fiber Selection and Standards Guide for Premises Networks*; Corning White Paper: New York, NY, USA, 2013.
7. Indra, A. *Industrial Fiber Optics in Train Transportation Systems*; Avago Technologies White Paper: San Jose, CA, USA, 2012.
8. Liu, S.; Xing, B.; Li, B.; Gu, M. Ship information system: Overview and research trends. *Int. J. Naval Arch. Ocean Eng.* **2014**, *6*, 670–684. [CrossRef]
9. Olson, E. The case for fiber in commercial aircraft: Solving the bandwidth/distance challenge. *Mil. Aerosp. Electron.* **2016**. Available online: <https://www.militaryaerospace.com/na/te-connectivity/the-case-for-fiber-in-commercial-aircraft.html> (accessed on 31 August 2018).
10. Bourdine, A.V. *Few-Mode Regime of Optical Signal Transmission over Multimode Optical Fibers: Applications in Modern Infocommunications*; PSUTI: Samara, Russia, 2011; ISBN 978-5-904029-22-7.
11. Buckler, M.J.; Kummer, R.; Mettler, S.C.; Miller, M. Fabrication of Optical Fibers Using Differential Mode-Group Delay Measurement. U.S. Patent 4286979, 1 September 1981.
12. Stone, F.T.; Ritger, A.J.; Head, E.D. The use of a quantitative differential mode delay technique to improve fiber bandwidth. *IEEE J. Lightwave Technol.* **1983**, *LT-1*, 585–587. [CrossRef]
13. Abbot, J.S.; Harsbarger, D.E. Laser Optimized Multimode Fiber and Method for Use with Laser and System Employing Same. U.S. Patent 2002/0197038, 12 August 2002.
14. Bangalore Krishnaswamy, P.; Dutta, S.; Panneerselvam, S.R.; Nageswaran, S.K. Optical Fiber Having Higher Bandwidth and Method for Producing the Same. Patent WO 2007/043060, 19 April 2007.
15. Golowich, S.E.; Jones, S.L.; Ritger, A.J.; Thornburg, K.S. Apparatus and Method for Improving Bandwidth of Multimode Fibers. U.S. Patent 6574403 B1, 3 June 2003.
16. Achten, F.J.; Jetten, M.P.M.; Krabshuis, G.-J.; Kuyt, G.; Matthijsse, P.; Van Stralen, M.J.N. New generation of broad wavelength window multimode fibres. In *Proceedings: ECOC 2004, 30th European Conference on Optical Communication (ECOC), Stockholm, Sweden, 5–9 September 2004*; Kista Photonics Research Center: Stockholm, Sweden, 2004; Volume 4, pp. Th 3.3.3-1–Th 3.3.3-3.
17. Adams, M.J. *An Introduction to Optical Waveguides*; John Wiley & Sons Ltd.: New York, NY, USA, 1981; ISBN 13 978-0-4712-7969-3.
18. Bogolyubov, A.N.; Krasilnikov, A.V.; Minayev, D.V.; Sveshnikov, A.G. Finite difference method for solution of the problem of waveguide system synthesis. *Math. Model.* **2000**, *12*, 13–24.
19. Bogolyubov, A.N.; Butkarev, I.A.; Sveshnikov, I.A. Synthesis of optical fibers. *Radiotekhnika* **2004**, *12*, 4–12.
20. Bourdine, A.V. Method for chromatic dispersion estimation of high-order guided modes in graded index single-cladding fibers. *Proc. SPIE* **2006**, *6605*, 660509-1–660509-13.
21. Bourdine, A.V. Modeling and simulation of piecewise regular multimode fiber links operating in a few-mode regime. *Adv. Opt. Technol.* **2013**, *2013*, 469389-1–469389-18. [CrossRef]
22. Snyder, A.W.; Love, J. *Optical Waveguide Theory*; Chapman & Hall: London, UK, 1983; ISBN 978-1-4613-2813-1.
23. Gradstein, I.S.; Ryjik, I.M. *Tables of Integrals, Series and Products*; GIFML: Moscow, Russia, 1963; ISBN 978-1-4832-6564-3.
24. Abramovitz, M.; Stegun, I.A. *Handbook of Mathematical Functions with Formulas, Graphs and Mathematical Tables*; Nauka: Moscow, Russia, 1979.

25. Bourdine, A.V.; Delmukhametov, O.R. Calculation of transmission parameters of the launched higher-order modes based on the combination of a modified Gaussian approximation and a finite element method. *Telecommun. Radio Eng.* **2013**, *72*, 111–123. [[CrossRef](#)]
26. Binh, L.N. *Design Guidelines for Ultra-Broadband Dispersion-Flattened Optical Fibers with Segmented-Core Index Profile*; Technical Report MECSE-14-2003; Monash University: Clayton, Australia, 2003.
27. Fleming, J.W. Dispersion in GeO₂-SiO₂ glasses. *App. Opt.* **1984**, *23*, 4486–4493.
28. Burdin, V.A. Methods for computation of Sellmeier coefficients for dispersion analysis of silica optical fibers. *Infocom Technol.* **2006**, *4*, 30–34.
29. Agrawal, G.P. *Nonlinear Fiber Optics*, 2nd ed.; Academic Press Inc.: San Diego, CA, USA, 1989; ISBN 13 978-0-1204-5142-5.
30. Yabre, G. Comprehensive theory of dispersion in graded-index optical fibers. *IEEE J. Lightwave Technol.* **2000**, *18*, 166–177. [[CrossRef](#)]
31. Yabre, G. Influence of core diameter on the 3-dB bandwidth of graded-index optical fibers. *IEEE J. Lightwave Technol.* **2000**, *18*, 668–676. [[CrossRef](#)]
32. Srapionov, V.A. Mode coupling at the splices of optical fibers with mismatched parameters. *Elektrosvyaz* **1985**, *10*, 10–12.
33. Bourdine, A.V. Mode coupling at the splice of diverse optical fibers. *Proc. SPIE* **2012**, *8787*, 878706-1–878706-12.
34. Bourdine, A.V.; Praporshchikov, D.E.; Yablochkin, K.A. Investigation of defects of refractive index profile of silica graded-index multimode fibers. *Proc. SPIE* **2011**, *7992*, 799206-1–799206-6.
35. Demidov, V.V.; Ter-Nersesyants, E.V.; Bourdine, A.V.; Burdin, V.A.; Minaeva, A.Y.; Matrosova, A.S.; Khokhlov, A.V.; Komarov, A.V.; Ustinov, S.V.; Golyeva, E.V.; et al. Methods and technique of manufacturing silica graded-index fibers with a large central defect of the refractive index profile for fiber-optic sensors based on few-mode effects. *Proc. SPIE* **2017**, *10342*, 103420X-1.
36. Raddatz, L.; White, I.H.; Cunningham, D.G.; Nowell, M.C. An experimental and theoretical study of the offset launch technique for the enhancement of the bandwidth of multimode fiber links. *IEEE J. Lightwave Technol.* **1998**, *16*, 324–331. [[CrossRef](#)]
37. Gowar, J. *Optical Communication Systems*; Pfentice/Hall International: London, UK, 1984; ISBN 13 638156-1.
38. Cunningham, D.; Nowell, M.; Hanson, D. Proposed Worst Case Link Model for Optical Physical Media Dependent Specification Development. IEEE 802.3z Task Force Presentation Materials, January 1997. Available online: http://www.ieee802.org/3/z/public/presentations/jan1997/dc_model.pdf (accessed on 31 August 2018).
39. Cunningham, D.; Nowell, M.; Hanson, D.; Kazovsky, L. The IEEE 802.3z Worst Case Link Model for Optical Physical Media Dependent Specification. IEEE 802.3z Task Force Presentation Materials, March 1997. Available online: <http://www.ieee802.org/3/z/public/presentations/mar1997/DCwpaper.pdf> (accessed on 31 August 2018).
40. Clarifying Optical Parameters, Power Budgets, and Fiber Plant Requirements for 10GBase-E and 10GBase-L. Cisco Systems White Papers 2005. Available online: https://www.cisco.com/c/en/us/products/collateral/interfaces-modules/10-gigabit-modules/prod_white_paper0900aecd8033fa80.pdf (accessed on 31 August 2018).

